Convective impact on temperatures observed near the tropical tropopause

STEVEN C. SHERWOOD

Department of Geology and Geophysics, Yale University, New Haven, CT, USA

TAKESHI HORINOUCHI

Radio Science Center for Space and Atmosphere, Kyoto University, Uji, Japan.

HEIDI A. ZELEZNIK

Department of Geology and Geophysics, Yale University, New Haven, CT, USA

ABSTRACT

Observed temperature trends and interannual variations near the tropical tropopause suggest that temperatures up to the cold point are controlled by the troposphere, but some models indicate otherwise. Here we extend previous investigations of thermal anomalies and heating profiles associated with tropical convective outbreak, by examining behavior near the tropopause. Observations show that active convective systems are locally associated with warm anomalies in the upper troposphere but cold anomalies in the lower troposphere and near the tropopause. Time-dependent solutions of Laplace's equations demonstrate that the cold anomaly below 100 hPa can be at least partly accounted for by adiabatic lofting associated with a transient heating pulse at lower levels. However, detailed examination of the cold-point tropopause in the data reveals that it moves against the lofting, downward toward higher pressure and colder potential temperatures, in response to convection. These variations qualitatively agree with longitudinal and ENSO-related variations in tropopause height and temperature reported in the literature, though seen here on hourly time scales. From this we infer local, mesoscale diabatic cooling of several K day^{-1} close to the tropopause during active convection. This exceeds the likely contribution from cloud-top radiative cooling, suggesting a role for convective turbulence in refrigerating the tropopause.

1. Introduction

There is no consensus as to what role, if any, convection plays in setting tropopause temperatures in the Tropics. The classical view is that the tropical cold point marks a division between convective and radiative control of the temperature profile (e.g. Held 1982). Convective control of temperatures is clearly evident in the lower and middle troposphere where lapse rates are quite close to moist adiabatic. However, temperature profiles begin to depart from the moist adiabat as low as 11 km while the tropopause does not occur until 16-17 km, leaving a disconcertingly large transition region between the two simple regimes. Recently, simple models have suggested that the cold point in the temperature profile is actually a stratospheric feature that has nothing to do with convection, owing its existence instead to the onset near 100 hPa of the photochemical production of UV-absorbing ozone (Kirk-Davidoff et al. 1999; Thuburn and Craig 2002). In these models, the convective tropopause and cold point are decoupled features. Here, we investigate this matter using observations and a model (we will refer to the region near 140-100 hPa generally as the "tropopause," and to the cold point—typically near 95 hPa— specifically as the "cold point tropopause").

The heat budget near the tropical tropopause is a topic of small but growing interest. This is because temperatures there are thought to control stratospheric water vapor and/or the prevalence of thin cirrus clouds, each of importance to climate. At present, we do not know how tropopause temperatures or cloud coverage will change if climate warms, for example. Further, recent observational studies have

Corresponding author address:
S. Sherwood, Yale University, New Haven, CT 06520 (ssherwood@alum.mit.edu)

found that well-known tropical disturbances, including the Madden-Julian oscillation, Kelvin waves, and others, are strongly expressed in the temperature and wind fields in the lower stratosphere, with striking, vertically varying structures (Straub and Kiladis 2002; Wheeler et al. 2000). While these expressions are likely to represent upward wave propagation initiated by tropospheric heating, there are surprising indications that tropical convective organization may in turn be influenced by stratospheric anomalies (Gray et al. 1992). In trying to make progress on the general subject of convective understanding and parameterization, it therefore behooves us to address the issue of convective effects at the highest levels.

Despite the aforementioned model results, a variety of observational evidence suggests that tropopause temperatures are indeed affected by tropospheric processes. First, radiative transfer calculations indicate that balance between radiative and large-scale advective sources of energy is not actually achieved until some distance above the cold point, with net radiative heating prevailing near the tropopause (Sherwood 2000a) especially if thin cirrus clouds contribute to the heating (Jensen et al. 1996). This implies a missing sink of energy near the tropopause, which may be either quasi-horizontal eddies, vertical convective transports of heat, or radiative cooling from cloud tops. Though models have sometimes found significant cooling due to eddies (e.g., Manabe and Mahlman 1976), observations do not indicate significant horizontal eddy fluxes of energy out of the tropics a these levels (Sherwood 2000a; White 1954). When vertical advection is taken into account, the implied time-averaged energy sink is even larger over the most intensively convective region of the tropics (Sherwood 2000a), suggesting a cooling mechanism there that is associated with deep convection.

Cold anomalies have been observed to appear rapidly near and above the cold-point tropopause over convective systems in the Indonesia region (Johnson and Kriete 1982), with suggested causes being adiabatic lifting, cloud-top radiative cooling, or turbulent mixing. On the other hand, Johnson (1986) observed in the same region a lowering of the tropopause and warming of the lower stratosphere with increasing cloud cover on *weekly* timescales, invoking nonlocal dynamical influences to explain this. A climatological connection between convection and tropopause temperatures was drawn by Reid and Gage (1981) on the basis of the fact that the mean and seasonal variation of the potential temperature at the tropical cold point closely matched those of the saturated equivalent potential temperature at the ocean surface. Further, variations in tropopause characteristics are coherent with ENSO (Randel et al. 2000; Reid and Gage 1985). In particular, the tropopause over Hawaii (distant from intense deep convection in either phase of ENSO) stays at the same potential temperature throughout the oscillation, while over a site in the Western Pacific, the tropopause potential temperature rises by several degrees during the ENSO warm phase when convection ordinarily found over the site moves east (Kiladis et al. 2001).

These observations imply a diabatic heat source at the tropopause that is negatively correlated with convective activity. However, no previous observations have been able to separate diabatic and adiabatic effects convincingly in explaining observed variations, nor isolate which diabatic effect (turbulent heat transport, cloud-top radiative cooling, or dynamically induced changes in radiative heating) is most important. Distinction of these mechanisms would be made easier by examining variations on convective time scales rather than the longer times scales relevant to most of the previous studies.

Due to the difficulty of modeling convection, observations must take center stage in addressing these questions. In this study, we extend the analysis of radiosonde data presented by Sherwood and Wahrlich (1999) up to 30 hPa using a modified analysis technique, paying particular attention to the tropopause. To gain insight into the diabatic effects and waves expected to occur in conjunction with convection, we employ the model of Horinouchi and Yoden (1996).

2. Radiosonde data analysis

a. Data and compositing/filtering methods

We begin with the 18-month set of radiosonde data from the Tropical Western Pacific region used by Sherwood and Wahrlich (1999), hereafter SW99. Those soundings were composited according to the growth or decay stage of local convection (if any), determined using hourly data from the GMS (Geostationary Meteorological Satellite) gathered within a 100-km square region surrounding the station. Sounding classification followed from the detection of convective "onset" and "termination" events based on the time progression of the amount of local cloud cover at temperatures below 208 K. Thus, soundings were classified in six categories numbered sequentially: 0 if no convection was present, 1 if an onset occurred within three hours after the sounding, 2 if an onset had occurred within the prior three hours, 3 if convection had been ongoing for at least three hours prior and afterward, 4 if a termination was coming up within three hours after the sounding, and 5 if a termination had occurred within the prior three hours. Readers should consult SW99 for further details.

Convection does not hover over sounding sites so as to facilitate easy compositing, but tends rather to propagate or advect past stations, typically steered by mid-level winds at rates of up to 10 $\mathrm{m\,s}-1$. Composites are based on the state of convection over the station at the observation time. The system's age category at that point may be determined either by observing the past and future cloudiness over the site (in which case a system moving in will be indistinguishable from one that sprung up locally), or by observing the evo-

lution of cloudiness in a region that moves with the system steering velocity. SW99 tried both and reported relatively small differences in the composites, occurring mainly in the final stage of convection. The results presented here do not depend significantly on which compositing technique is used.

The SW99 results showed warming and moistening anomalies in the upper troposphere during active convection, with cooling developing in the lower troposphere by stage 3, and finally a dry anomaly near the surface that developed as convection was decaying (stages 4-5). These anomalies corresponded generally with those expected from known features of tropical convective systems. The warm anomaly was present even before the onset of convection, indicating that it is part of a wave that organizes convection on time and/or space scales longer than those of the individual systems as defined by the compositing procedure. This illustrates the subtlety of the problem and the importance of accounting for nonlocal influences on the thermal state.

While the SW99 study reported moisture, this could not be extended above 300 hPa due to sensor failure above this level. Thus we do not consider moisture at all here. SW99 included winds in their study but did not closely examine them; here, we use zonal wind observations as a marker of waves generated by convection. We also determine a cold point temperature and pressure for each sounding.

The SW99 analysis did not quite reach the tropopause level, owing to reduced data quantity and noise associated with temporal and horizontal temperature variations which become significant as one approaches the tropopause. To address this problem, we have filtered the temperature, pressure, and cold point data according to Sherwood (2000c). Specifically, the measured quantities at a given level from a large set of tropical stations are fitted to a compact set of basis functions representing large-scale variations:

$$Z = \mu + \epsilon,$$

where μ is the expectation value at each station given the remaining data and a model including only empirically derived, slow/large-scale variations. This is done separately for each season, so seasonal variations are implicitly removed as well. Anomalies due to the influence of nearby convection will be contained in the "residual" ϵ; seasonal, intraseasonal, interannual, and horizontal variations, which would contribute noise to the composites, will appear in μ. For temperatures below 250 hPa, we retain the anomaly results already published in SW99 since the filtering procedure has very little effect. For temperatures at 250 hPa and above (which we will call the UT/LS or upper troposphere/lower stratosphere), for winds at all levels, and for cold-point characteristics, we will use ϵ to measure the local effects of convection. We note that this filtering procedure also removes atmospheric tides, which may have an amplitude of several tenths of a degree near the tropical tropopause (Swinbank et al. 1999).

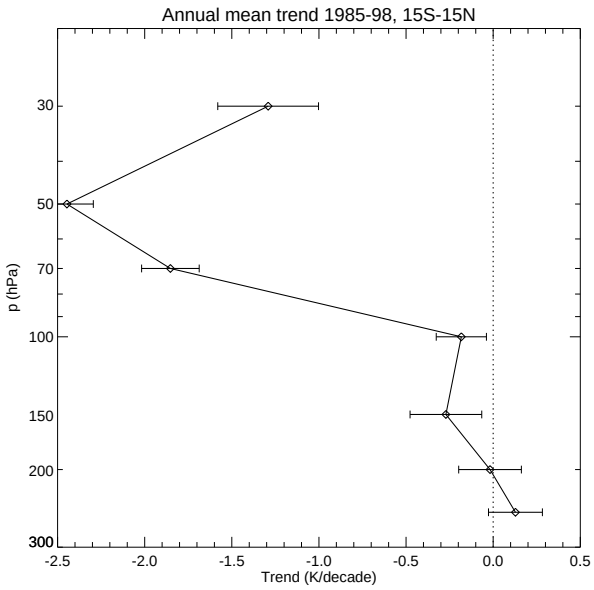

FIG. 1. The temperature trend vs. height between 15N-15S during the period 1985-98, from radiosonde data analyzed at mandatory reporting levels as described in text.

In performing the above procedure for winds and cold-point characteristics, we use a data set of 60 stations in the Western Pacific area that includes the nine used in Sherwood and Wahrlich (1999), with data collected from 1992-98. By including the extra stations and time period, the model μ may be determined more accurately from the data by the procedure. For UT/LS temperatures, we use the even larger dataset of 15-year duration and 137 stations throughout the tropics presented in Sherwood (2000c). Though sensitivity tests indicate that the smaller dataset is sufficient, our reason for using the larger temperature dataset is to be able to show trends. For each variable, our model for μ is as described in Sherwood (2000c), except that for temperature we have also included a trend term at each station.

b. UT/LS temperature trends

The 1985-99 dataset demonstrates an interesting trend characteristic. We obtain a mean 15N-15S temperature trend by optimal interpolation of the trend observed at each station, taking into account the varying uncertainty of each station's trend, as described in Sherwood (2000b). The result is shown in Fig. 1. A strong cooling trend over this particular 15-year period is clearly evident in the stratosphere; it is stronger than the longer-term cooling trend (Angell 2000). The reason for this unusual trend is not clear. However, the trend is completely gone by the 100 hPa level where it is indistinguishable from that at lower levels.

This similarity between 100-hPa and tropospheric trends—even in the face of substantial change in the lower stratosphere—

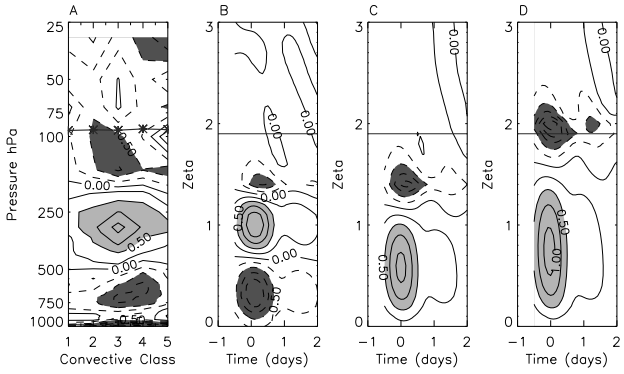

FIG. 2. (a) Composite temperature profile of mean residual ϵ (at 250 hPa and above) or mean temperature (at 300 hPa and below) vs. stage of convection from radiosonde data. Peak convective activity corresponds to stage 3; typical time scale from beginning to end is $\sim$1 day. (b-d) Evolution of temperature according to the wave model, with (b) bimodal heating to $\zeta = 1.4$ peaking at 10 K/day; (c) unimodal heating to $\zeta = 1.4$ peaking at 20 K/day, and (d) unimodal heating to $\zeta = 1.9$ (the "tropopause" height, where stability increases) peaking at 30 K/day. Contour interval is 0.25 K.

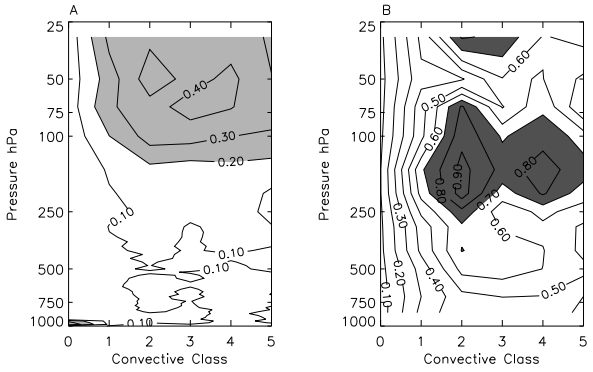

FIG. 3. The 1-sigma uncertainties of the sounding composite results shown in (a) Fig. 2a (values above 0.20 K shaded) and (b) Fig. 4a (values above 0.70 m/s shaded).

reinforces the connections between thermal characteristics near the cold-point (usually only slightly above the 100 hPa level) and the surface, previously reported on ENSO and annual time scales. Although it is possible that a decadal radiative heating variation occurred that was sharply confined to the stratosphere, and that similar coincidences explain the behavior on the other time scales, the overall pattern suggests that tropospheric processes of some kind are in firm control of the temperature at least to 100 hPa which is virtually all the way to the cold point.

c. Composite anomalies

The composite temperature profile over the six stages is shown in Fig. 2a, while the 1-sigma uncertainty is shown in Fig. 3a. In addition to the features pointed out by SW99, a cold feature appears that extends from about 200-100 hPa, similar to features found in a variety of convectively-coupled waves (Straub and Kiladis 2002; Wheeler et al. 2000). Above the tropopause we see a less clear signal whose statistical significance is marginal. The composite zonal wind profile (Fig. 4a) shows a predominantly easterly anomaly at most levels, especially in the upper troposphere, beginning prior to the onset of convection but intensifying significantly during the convection.

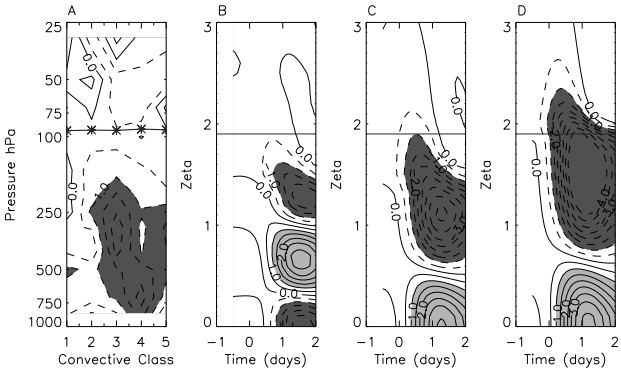

FIG. 4. As in Fig. 2, except zonal wind velocity. Contour interval is 0.5 m/s.

3. Model investigation

a. Description of model

The dynamical response of the atmosphere to heating can be represented as a sum of excited waves, which propagate

vertically and horizontally away from the heating source and are damped mechanically and radiatively. By using a simple numerical model, we examine the adiabatic temperature change above the heating in order to help interpret the observations.

The model used is identical to that used by Horinouchi and Yoden (1996; HY96) and Sobel and Horinouchi (2000) except for the resolution and tropopause height assumed. It computes the linear response to prescribed diabatic heating in the spherical geometry by using an expansion in Hough modes, as is done in the classical tidal calculation. The Hough modes are derived using spherical harmonics with rhomboidal truncation at R120. The basic state is at rest with two layers of different static stability, representing the troposphere and stratosphere, divided at $\zeta = 1.9$. The vertical coordinate $\zeta \equiv -\log(p/p_0)$, where p is pressure and p_0 is a constant, so ζ is approximately equivalent to a nondimensional altitude. The vertical boundary conditions are the linearized free slip at $\zeta = 0$ and the radiation condition at $\zeta = +\infty$. As the dumping mechanism, the model has Newtonian cooling with an e-folding time of 20 days. See HY96 for more details.

The diabatic heating imposed is sinusoidal in vertical, and Gaussian in time and horizontal:

$$Q = \begin{cases} Q_0\, e^{\zeta/2} \sin(\pi\zeta/\zeta_S) \exp\left[-\frac{\lambda^2}{2\Lambda^2} - \frac{(\varphi-\varphi_0)^2}{2\Phi^2} - \frac{t^2}{2T^2}\right] & \text{for } 0 \le \zeta \le \zeta_T \\ 0 & \text{for } \zeta > \zeta_T \end{cases} \tag{1}$$

where λ, φ, and t are longitude, latitude, and time, respectively. We set both horizontal scales to 4°, approximately equal to the decorrelation length scale of daily outgoing longwave radiation anomalies according to Smith and Rutan (1994), and we set the time scale T to 10 hours, typical of the decay time of active convection for this size system according to Sherwood and Wahrlich (1999). The latitude of the center of the heating is set to 6°N, which is near the centroid of the available sounding data. Cases run with heating centered at the equator or with different spatial and temporal scales did not differ significantly in the responses we will examine, so we do not show them. For comparison with observations, we sample the model output near the peak heating over a time and spatial domain similar to that of the sounding observations with respect to the observed convective systems. For the experiments described here, the constant Q_0 is set to 20 K day^{-1}.

The vertical variation of heating is described by a top ζ_T and a half-wavelength ζ_S. We have run the model with three heating profiles as shown in Fig. 5. The bimodal profile approximates heating associated with the stratiform outflow of a convective system, while the monomodal profiles approximate the heating associated with the convective portion (e.g. Mapes and Houze 1995). The heating is similar to that used by HY96 and Sobel and Horinouchi (2000). See these papers for the basic dynamics of the response.

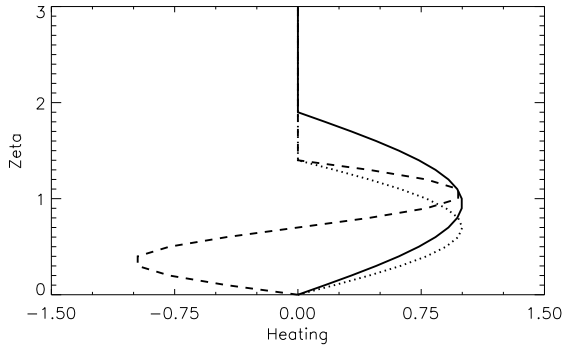

FIG. 5. Heating rates in the three model runs.

b. Simulated vs. observed temperature perturbations

The model simulated temperature perturbation is indicated in Fig. 2b-d for the three idealized heating profiles. In each case, the heating and cooling regions are accompanied by warm and cool anomalies. The thermal anomalies lag the heating slightly, by about three hours in the bimodal and 1.5 hours in the unimodal cases. In addition, an upper-level cool anomaly appears sandwiched between the top of the heating and the tropopause, where no diabatic cooling occurs. This feature actually extends somewhat below the height of zero heating, with the zero perturbation level located near $\zeta = 1.2, 1.6$ for unimodal heating top at $\zeta = 1.4, 1.9$ respectively. So before it reaches zero, the heating becomes too weak to balance the adiabatic cooling driven by the greater heating at lower levels. This is likely to be sensitive to the shape of the heating profile, which is confirmed by noting that it is much less apparent with the bimodal profile (Fig. 2b) than with the unimodal ones. The cool anomaly continues through the tropopause in the deepest heating case, but does not reach the tropopause in either of the shallower heating cases.

Comparing the modeled and observed results in Fig. 2 shows that the key features are well captured by the models, if one allows for uncertainty in the best location for placement of the top of heating and if one reckons that the convective stages unfold over a typical time period of somewhat less than one day. The observations are best accounted for by a heating profile that includes a unimodal component topping out somewhere in between those shown at $\zeta = 1.4$ and 1.9, and a strong bimodal component topping out near or slightly above $\zeta = 1.4$. The implied heating profile is concentrated mainly in the upper troposphere, as indicated in observational studies of stratiform heating in mesoscale convective systems (e.g. Mapes and Houze 1995). One possibly important discrepancy between the models and observations is the slightly greater extent of the observed near-tropopause cool anomaly in the observations. However, this difference is not large

enough to inspire confidence without further investigation.

Our results are qualitatively similar to those of Johnson and Kriete (1982), who found rather large (6-10 K) peak cooling anomalies above the cold-point tropopause in a sampling of three wintertime convective systems near Indonesia. The height of those anomaly peaks suggests that the difference found here between observed and modeled anomalies could be larger in the Indonesia region, although it may not be safe to generalize from cases observed over only a few days. It is also possible that tidal effects contributed to their signal. The dynamical, multi-day warming event observed by Johnson (1986) at a time of enhanced convection does not appear in our composites, so the connection noted there may not be systematic.

The one-sigma uncertainties in the plotted values appear in Fig. 3a. These uncertainties are around 0.1 K in the troposphere—indicating strong significance of the main tropospheric anomalies—but approach 0.5 K in the lower stratosphere, indicating that the anomalies found there in Fig. 2a are not significantly different from zero at acceptable levels of confidence.

c. Zonal winds

The corresponding zonal wind anomalies are shown in Fig. 4. Here, the agreement is poor. Easterlies show up in the observations at nearly all levels, peaking at about the same time that the warming anomalies are greatest, but this is not predicted by the model in any of its configurations. Instead, the model predicts winds that do not really get going until after the temperature anomalies have largely subsided, whereupon strong winds develop that are easterly where the heating decreases with height and westerly where heating increases with height. This latter result is expected due to the variation of Coriolis parameter with latitude, appearing in the well-known solution of Gill (1980) for the baroclinic response to steady localized heating.

So it is not obvious where the observed easterly anomalies, with their significant barotropic component, are coming from. They are probably associated with synoptic and planetary-scale convectively coupled dynamics that are not simulated by our model. Inspection of, for example, Figure 16 in Straub and Kiladis (2002) shows that in their central Pacific disturbances, easterly winds in the upper troposphere north of the equator coincided with convection, offset only slightly to the east but with considerable overlap. That flow pattern was associated with an evolving wave and was not driven purely by local heating. The waves propagated rapidly with time scales of a few days, long enough for the wind field to adjust to the changing mass field (including contributions from nonlocal heat sources) but short enough that such disturbances would not have been removed by our data filtering procedure. The convectively coupled Kelvin waves of Straub and Kiladis (2003) showed wind anomalies of order 1 $\mathrm{m\,s^{-1}}$ relative to temperature anomalies of order 0.1 K; MJO composites show similar or greater ratios of wind to thermal anomalies (G. Kiladis, pers. comm, 2002). Such large wind-to-temperature ratios are characteristic of geostrophically balanced disturbances at low latitudes, but are much greater than the approximately 1 $\mathrm{m\,s^{-1}}$ per K anomaly observed in our composite. One possible reason for this is discussed below.

The large amplitude, and inherent nonlocality in time and space, of balanced wind anomalies in the tropics forces us to conclude that our observed wind composites will not faithfully represent the response to local heating, even with the filtering techniques that we have used to eliminate intraseasonal and longer variations. We tried subjecting the data to high-pass filtering by subtracting out the mean obtained from a 30-day averaging window. This made little difference, indicating that the wind anomalies result from organization occurring on time scales of no more than a week or two. We also tried compositing the unfiltered wind, which showed more erratic anomalies but with no significant qualitative difference. Beyond establishing their synoptic origins, we make no further effort to interpret these wind anomalies here.

d. Wave superposition and the lower stratosphere

The Kelvin wave composites of Straub and Kiladis (2003, 2002) were remarkable in showing temperature and wind anomalies of equal or greater magnitude in the stratosphere as in the troposphere. By contrast, the simulated and observed anomalies in Fig. 2 are much weaker in the stratosphere than in the troposphere. For the simulated anomalies, this is expected, since the waves propagate horizontally as well as vertically so that local stratospheric anomalies could only come from remote forcing not included in the simulation. But in the observations, two-way coupling between waves and convection might have been expected to yield signals at all levels.

A way of understanding the failure of these to appear lies the the principle of wave interference. Fig. 6 shows the model results broken down by wave type (Kelvin, Rossby, and other gravity waves). Each wave type contributes significantly to the model response near the heating, though the waves have widely varying propagation characteristics (most waves propagate horizontally and vertically, though the Rossby waves include vertically evanescent Hough modes). Near the time and location of peak heating, all contributions are in phase, but incoherence causes the magnitude of average response to decrease elsewhere—for example, in the stratosphere. This behavior is expected all the more when we consider that each wave type occurs over a wide range of zonal and vertical wavenumbers.

We expect each wave type to be rattling around in the

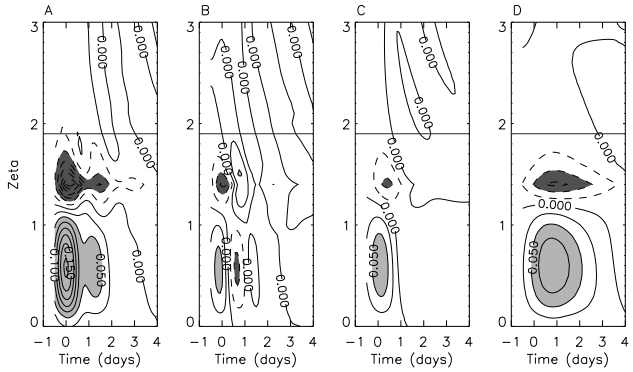

FIG. 6. Model response to heating up to $\zeta = 1.4$, broken out by wave type: (a) All waves, (b) gravity waves (not including Kelvin waves), (c) Kelvin waves, and (d) Rossby waves.

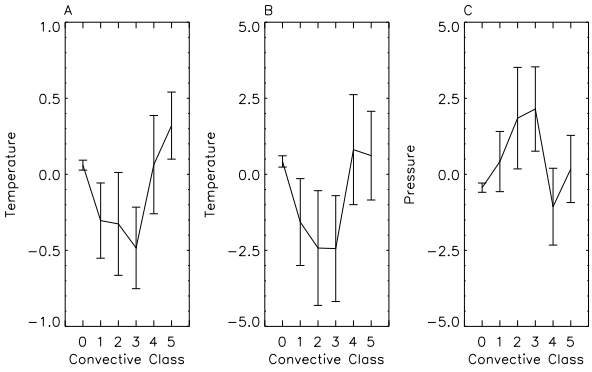

FIG. 7. Composite cold point properties at each convective stage: (a) temperature in K, (b) potential temperature in K, and (c) pressure in hPa. Error bars show standard error due to sampling.

Tropics due to remote forcing, and that all of these waves will have influenced convection in our sampling domain. If filtering is not performed to select specific wave types, a composite over many convective systems will decay rapidly into noise with distance (in time or space) from the compositing event, due to the many discordant influences implicitly being included. By contrast, the analysis technique employed by Wheeler et al. (2000) isolated particular regions of phase space, obtaining pure waves that were expressed at all levels without prejudice.

An extension of the superposition argument offers an explanation of the relative weakness of the observed tropospheric zonal wind signals. While heating and temperature anomalies are connected directly by local mechanisms, the wind adjustment is nonlocal and its relationship with temperature will differ among various waves, yielding an average wind that is relatively weak compared to what one would see in a pure wave. The fact that there is an association between active convection and easterly anomalies having a synoptic, largely barotropic nature, and that the association survives this averaging process, is an interesting result with no obvious explanation.

4. The cold point

In the composites, the observed cooling tendency near the tropopause appeared somewhat larger than the adiabatic cooling calculated in the model. Here, we reexamine the important matter of thermal effects at the cold point.

Over the western Pacific region, the cold point is usually a sharp feature, i.e., the vertical derivative of temperature is often nearly discontinuous. In this case, the cold point will remain on the same material surface regardless of how the air mass containing the tropopause is lofted or subsides, provided that the vertical motions are adiabatic and vertically continuous through the cold point. Thus, the cold point pressure $p_{\rm cp}$ and potential temperature $\theta_{\rm cp}$ can be used as markers of adiabatic lifting and diabatic heating, respectively, giving us another way to distinguish these influences on temperature at the cold-point level. Possible problems with this strategy, which do not appear to be significant, are investigated in Section 4a.

Having identified $T_{\rm cp}$, $\theta_{\rm cp}$, and $p_{\rm cp}$ in all soundings, it is straightforward to composite these variables by convective stage. Figure 7 shows these composites. Remarkably, both $T_{\rm cp}$ and $\theta_{\rm cp}$ dip during convection in a very similar manner, rising again during the stratiform phase of the system. Pressure anomalies are negatively correlated with those of temperature, actually rising during the time that $T_{\rm cp}$ and $\theta_{\rm cp}$ are low, indicating that the cold point temperature changes *cannot have been adiabatic*. The statistical significance of this counterintuitive correlation is much stronger than that of the individual anomalies at the various stages. Fig. 8 contrasts the adiabatic and observed alteration of the cold point. The return of temperatures to normal during the decay of the system is not unexpected, given that horizontal wind speeds of order 10 m s^{-1} will sweep uncooled air into the sampling region ($\sim$100 km on a side) within a few hours once the cooling process has ceased.

The degree of diabatic cooling follows directly from the variations in $\theta_{\rm cp}$, which when rescaled by the Exner function indicate diabatic cooling of about 1 C in the time span of a few hours. We may convert this figure into a crude area-mean cooling rate by noting that roughly 2% of the soundings in the dataset were classified as onset soundings, and that the soundings were spaced 3 hours apart. Dividing yields a repeat period of about 6 days, which with a 1 C temperature drop per event yields a time-averaged diabatic cooling of about 0.2 K day^{-1}. The uncertainty of this estimate is large, due to the sampling uncertainty as well as the crude reckoning.

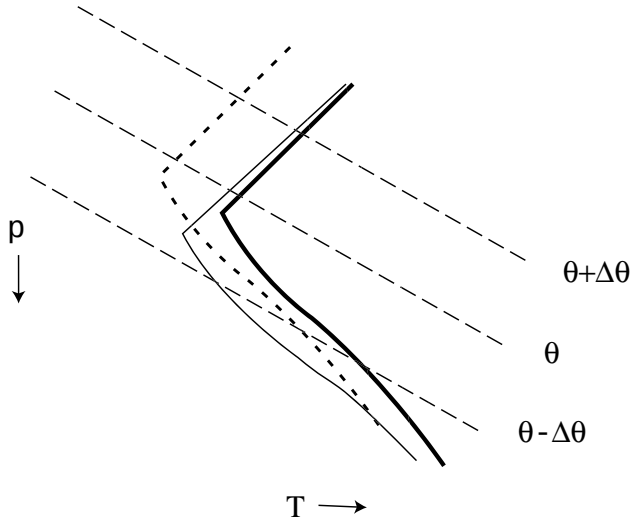

FIG. 8. Diagram showing changes in tropopause during convection. Thick solid line is the initial state, short dashed line is the state that would follow an adiabatic lofting, while thin solid line is the observed change. Straight dashed lines denote constant potential temperature contours.

a. Could adiabatic variations move the cold point relative to material surfaces?

Our proposition that the cold point remains on a material surface is assured only if the vertical derivative of lapse rate at the cold point is sufficiently large compared to that of any vertical velocity fluctuations. This is not guaranteed since the cold point is not always sharp. Gravity waves near the tropopause can have short vertical wavelengths, allowing the possibility of sufficiently rapid vertical variation in adiabatic cooling so as to shift the material location of the coldest point. Further, soundings commonly exhibit multiple secondary minima in temperature (sometimes called multiple cold-point tropopauses) that may be almost as cold as the "cold point." An adiabatic motion might cool these more than the original cold point, potentially shifting the cold point to a different material surface (though the increase of stability with height means that such a shift would naturally tend to be *upward*, in contrast to observations, unless the lofting motion decreased rapidly with height).

To see whether such affects contributed to our results, we performed the following test. We supposed as a "null hypothesis" that all deviations of convective soundings from the non-convective mean were purely adiabatic, calculating the pressure change that would have been required to explain the deviation of each data point from the non-convective profile. These putative displacements were then backed out of the convective soundings by applying an adiabatic pressure and temperature change to each data point to bring it back onto the non-convective reference profile. Cold points were then re-assigned and their properties re-composited from the original data using the new assignments. In only a few cases did the assignment differ, and the resulting composites were essentially unchanged, demonstrating that adiabatic motions could not have caused sufficient material displacements of the cold point to affect our results.

b. Cloud top cooling?

The appearance of the 1 C diabatic anomaly within a few hours indicates a mesoscale mean cooling rate on the order of 5-10 K day^{-1} during active convection. It is difficult to obtain this cooling rate from radiation alone. It is often argued that infrared cooling from cloud top can lead to significant cooling in a thin layer near the cloud top. This is true for clouds in the lower and middle troposphere, but close to the tropopause, the cooling potential of this mechanism is reduced by the low radiating temperatures. Further, the proximity to incoming sunlight increases the offsetting solar heating effect. The upper limit of the net infrared flux difference above and below the cooling skin at the top of an optically thick cloud is simply

$$\delta F_{\mathrm{IR}} = \sigma T^4$$

where T is the cloud top temperature. This result holds exactly only if there is no stratospheric emission and if the cloud is so thick that upward emission below cloud top is at the same temperature as the cloud top. For $T = 200\,\mathrm{K}$ we have $\delta F_{\mathrm{IR}} = 90\ \mathrm{W\,m^{-2}}$; for $T = 195\,\mathrm{K}$, $\delta F_{\mathrm{IR}} = 82\ \mathrm{W\,m^{-2}}$. If the cloud is so thick that no sunlight penetrates it then, since observations and models show maximum albedos of around 0.7 for ice clouds, the net solar flux convergence into the cloud will be at least $340 \times 0.3 = 102\ \mathrm{W\,m^{-2}}$ for global mean insolation, or $131\ \mathrm{W\,m^{-2}}$ with diurnal mean equatorial insolation. In other words, for infinitely thick clouds occurring at random times of day in the Tropics, the cloud top would heat rather than cool! However, clouds are never infinitely thick, and solar absorption occurs lower than infrared emission.

Thus we have used the CCM3 radiative transfer model to calculate cloud-top cooling rates with thick cloud tops at the cold-point level (if tops are below the cold point level, the net diabatic effect is insignificant). The cold point was 200 K. With a cloud of 1000 g m^{-2} total water content distributed evenly in model layers from the cold point down to the freezing level (a total optical depth of about six in each model layer), the net infrared flux difference above and below the cold point layer was 78 W m^{-2}, sufficient to give an infrared cooling of up to 51 K day^{-1} if all cooling were concentrated into one kilometer. The diurnal mean solar heating at tropical latitudes in such a circumstance was calculated by the model to be 44 K day^{-1}, leaving a net cooling of only 7 K day^{-1}. This is assuming that CCM3 has realistic solar absorption, though the omission of 3-D effects and other absorption enhancements means that the true solar

absorption might be closer to, or perhaps even greater than, the longwave emission. Further, since only the convective cores have any chance of reaching the cold point, and these typically occupy only a small fraction of the cloudy area, a realistic cooling rate within the mesoscale regions used in making the observed composites would be perhaps an order of magnitude less than for total coverage, or less than one K day^{-1} even without worrying about the sufficiency of solar absorption. Finally, cloud-top cooling would probably be spread over more than one kilometer in the vertical since cloud top heights would vary by more than that, reducing the temperature tendencies at any given point even further. Reasonable changes to the cloud water distribution in CCM3 did not substantially alter the net result, except that even less cooling occurred when insufficient cloud water was included in the upper model layer to render it opaque in the infrared (which would include, for example, the case of optically thin cirrus clouds overlying a thick anvil).

5. Conclusion

Our analysis of radiosonde data indicates that convection over the Tropical Western Pacific generates cold anomalies above the heating, due at least in part to adiabatic lofting caused by heating in the main troposphere. This cooling occurs from about 150-100 hPa. We were not able to distinguish systematic temperature effects above this, due to noise in the data, but were able to establish that they were not as large as temperature changes appearing in Kelvin, Rossby and other wave composites that have been isolated in previous investigations. This is probably because many wave types and scales superpose constructively only where the heating is, becoming incoherent in the stratosphere leading to smaller mean contributions when composited in the way we have done.

We argue that heating may be examined more closely near the cold point by using the latter to identify motions of material surfaces under the hypothesis that changes are purely adiabatic. We find that the results are inconsistent with purely adiabatic lofting, and that time-mean diabatic cooling of order 0.2 K day^{-1} must be occurring close to the cold point, or 5-10 K day^{-1} when convection is most active.

Specifically, the passage of a convective system leads to a rapid (within a few hours) drop of the cold point to a lower material surface and higher pressure. The new cold point is slightly colder, but possesses significantly less potential temperature ($\sim$2 K lower) and dry static energy than did the cold point prior to convection. These results indicate that diabatic cooling just below the old cold point altitude chills the air to a temperature below that of the original cold point, establishing a new one. This result stands in contrast to what one might initially expect—that convection will tunnel deeper into the stratosphere—but helps to explain previous observations that the cold-point tropopause tends to occur at a higher pressure in regions of more active convection (e.g., Seidel et al. 2001), and that its pressure tends to fall over the Western Pacific during ENSO warm events (Kiladis et al. 2001). The result also makes sense from a climatological perspective, in that rising motion outside of convective events would tend to loft the cold point to higher altitudes, requiring some mechanism of reestablishing cold points at lower levels or moving them downward in convection in order to maintain equilibrium.

Though we cannot establish definitively the reason for the diabatic cooling, we believe cloud-top radiative effects are unable to account for it due to the rapidity with which it develops. Instead, the most likely explanation is insertion of cold air by penetrative cumulus clouds (Sherwood 2000a). If so, the numbers given here would likely be smaller over other ocean regions, but perhaps larger over continental regions that have more intense convection. At any rate, we believe these results provide strong evidence that convection really does play a dominant role in establishing the location and temperature of the tropical cold point, contrary to the implications of some idealized climate models. Further work with cloud resolving models will be important in shedding further light on convective effects near the tropopause.

Acknowledgments. We thank Adam Sobel, Lenny Pfister, and George Kiladis for helpful discussions that led to improvements in this study. This work was supported by NASA EOS/IDS grant NAG-59632 and NSF grant ATM-0134893.

REFERENCES

Angell, J. K., 2000: Difference in radiosonde temperature trend for the period 1979-1998 of MSU data and the period 1959-1998 twice as long. *Geophys. Res. Lett.*, **27**, 2177–2180.

Gill, A. E., 1980: Some simple solutions for heat-induced tropical circulation. *Q. J. R. Meteorol. Soc.*, **106**, 447–462.

Gray, W. M., J. D. Sheaffer, and J. A. Knaff, 1992: Hypothesized mechanism for stratospheric QBO influence on ENSO variability. *Geophys. Res. Lett.*, **19**, 107–110.

Held, I. M., 1982: On the height of the tropopause and the static stability of the troposphere. *J. Atmos. Sci.*, **39**, 412–417.

Horinouchi, T., and S. Yoden, 1996: Excitation of transient waves by localized episodic heating in the tropics and their propagation into the middle atmosphere. *J. Meteorol. Soc. Jpn.*, **74**, 189–210.

Jensen, E. J., O. B. Toon, H. B. Selkirk, J. D. Spinhirne, and M. R. Schoeberl, 1996: On the formation and persistence of subvisible cirrus clouds near the tropical tropopause. *J. Geophys. Res.*, **101**(D), 21,361–21,375.

Johnson, R. H., 1986: Short-term variations of the tropopause height over the winter MONEX area. *J. Atmos. Sci.*, **43**, 1152–1163.

Johnson, R. H., and D. C. Kriete, 1982: Thermodynamic and circulation characteristics of winter monsoon tropical mesoscale convection. *Mon. Weather Rev.*, **110**, 1898–1911.

Kiladis, G. N., K. H. Straub, G. C. Reid, and K. S. Gage, 2001: Aspects of interannual and intraseasonal variability of the tropopause and lower stratosphere. *Q. J. R. Meteorol. Soc.*, **127**, 1961–1983.

Kirk-Davidoff, D. B., E. J. Hintsa, J. Anderson, and D. W. Keith, 1999: The effect of climate change on ozone depletion through changes in stratospheric water vapour. *Nature*, **402**, 399–401.

Manabe, S., and J. D. Mahlman, 1976: Simulation of seasonal and interhemispheric variations in stratospheric circulation. *J. Atmos. Sci.*, **33**, 2185–2217.

Mapes, B. E., and R. A. Houze, 1995: Diabatic divergence profiles in western Pacific mesoscale convective systems. *J. Atmos. Sci.*, **52**, 1807–1828.

Randel, W. J., F. Wu, and D. J. Gaffen, 2000: Interannual variability of the tropical tropopause derived from radiosonde data and ncep reanalyses. *J. Geophys. Res.-Atmos.*, **105**, 15,509–15,523.

Reid, G. C., and K. S. Gage, 1981: On the annual variation in height of the tropical tropopause. *J. Atmos. Sci.*, **38**, 1928–1938.

Reid, G. C., and K. S. Gage, 1985: Interannual variations in the height of the tropical tropopause. *J. Geophys. Res.-Atmos.*, **90**, 5629–5635.

Seidel, D. J., R. J. Ross, J. K. Angell, and G. C. Reid, 2001: Climatological characteristics of the tropical tropopause as revealed by radiosondes. *J. Geophys. Res.-Atmos.*, **106**, 7857–7878.

Sherwood, S. C., 2000a: A stratospheric "drain" over the maritime continent. *Geophys. Res. Lett.*, **27**, 677–680.

Sherwood, S. C., 2000b: Climate signal mapping and an application to atmospheric tides. *Geophys. Res. Lett.*, **27**, 3525–3528.

Sherwood, S. C., 2000c: Climate signals from station arrays with missing data, and an application to winds. *J. Geophys. Res.*, **105**, 29,489–29,500.

Sherwood, S. C., and R. Wahrlich, 1999: Observed evolution of tropical convective events and their environment. *Mon. Weather Rev.*, **127**, 1777–1795.

Smith, G. L., and D. Rutan, 1994: Spatial variability of outgoing longwave radiation. *J. Atmos. Sci.*, **51**, 1808–1822.

Sobel, A. H., and T. Horinouchi, 2000: On the dynamics of easterly waves, monsoon depressions, and tropical depression type disturbances. *J. Meteor. Soc. Japan*, **78**, 167–173.

Straub, K., and G. Kiladis, 2003: The observed structure of convectively coupled Kelvin waves: comparison with simple models of coupled wave instability. *J. Atmos. Sci.*, **0**. In Press.

Straub, K. H., and G. N. Kiladis, 2002: Observations of a convectively coupled Kelvin wave in the eastern Pacific ITCZ. *J. Atmos. Sci.*, **59**, 30–53.

Swinbank, R., R. L. Orris, and D. L. Wu, 1999: Stratospheric tides and data assimilation. *J. Geophys. Res.*, **104**, 16,929–16,941.

Thuburn, J., and G. C. Craig, 2002: On the temperature structure of the tropical substratosphere. *J. Geophys. Res.*, **107**, 10.1029/2001JD000,448.

Wheeler, M., G. N. Kiladis, and P. J. Webster, 2000: Large-scale dynamical fields associated with convectively coupled equatorial waves. *J. Atmos. Sci.*, **57**, 613–640.

White, R. B., 1954: The counter-gradient flux of sensible heat in the lower stratosphere. *Tellus*, **6**, 177–178.

Printed May 5, 2003.